Doping dependence of spin-lattice coupling and two-dimensional ordering in multiferroic hexagonal $Y_{1-x}Lu_xMnO_3$ ($0 \le x \le 1$)

Junghwan Park,[1,2,3] Seongsu Lee,[2,*] Misun Kang,[2] Kwang-Hyun Jang,[2] Changhee Lee,[4] S. V. Streltsov,[5,6] V. V. Mazurenko,[6]
M. V. Valentyuk,[6] J. E. Medvedeva,[7] T. Kamiyama,[8] and J.-G. Park[1,2,3,9,†]

[1]*Center for Strongly Correlated Materials Research, Seoul National University, Seoul 151-742, Korea*
[2]*Department of Physics, Sungkyunkwan University, Suwon 440-746, Korea*
[3]*Department of Energy Science, Sungkyunkwan University, Suwon 440-746, Korea*
[4]*Neutron Science Division, Korea Atomic Energy Research Institute, Daejon 305-600, Korea*
[5]*Institute of Metal Physics, S. Kovalevskoy Street 18, 620041 Ekaterinburg GSP-170, Russia*
[6]*Ural State Technical University, Mira Street 19, 620002 Ekaterinburg, Russia*
[7]*Missouri University of Science and Technology, 1315 N. Pine Street, Rolla, Missouri 65409, USA*
[8]*Institute of Materials Structure Science, KEK, Tsukuba 305-0801, Japan*
[9]*Department of Physics & Astronomy, Seoul National University, Seoul 151-742, Korea*
(Received 4 February 2010; revised manuscript received 26 July 2010; published 26 August 2010)

We have examined a complete phase diagram of $Y_{1-x}Lu_xMnO_3$ with $0 \le x \le 1$ by using bulk measurements and neutron-diffraction studies. With increasing Lu concentration, Curie-Weiss temperature and Neel temperature are found to increase continuously while the two-dimensional nature of short-range magnetic correlation persists even in the paramagnetic phase throughout the entire doping range. At the same time, the lattice constants and the unit-cell volume get contracted with Lu doping, i.e., chemical pressure effect. This decrease in the lattice constants and the unit-cell volume then leads naturally to an increased magnetic exchange interaction as found in our local spin-density approximation band calculations. We also discover that there is strong correlation in the temperature dependence of a volume anomaly at T_N and the magnetic moments.

I. INTRODUCTION

Coexistence of ferroelectric and magnetic phases is a relatively rare phenomenon, at least until quite recently, among natural materials with only a limited number of compounds showing this so-called multiferroic behavior.[1,2] However, despite the scarcity in nature the field has attracted considerable amount of interests because they offer a rare opportunity, where the two seemingly independent phenomena are coupled to one another enabling one to explore the unusual coupling of the two effects.[3] One such rare example of the multiferroic materials is hexagonal manganites $RMnO_3$ with space group $P6_3cm$ for elements at the rare-earth (R) site with a relatively small ionic radius: Ho, Er, Tm, Yb, Lu, Y, Sc, and In.[4] Another interesting point about the hexagonal manganites is that the Mn ions form a natural two-dimensional (2D) edge-sharing triangular network, which becomes magnetically frustrated with an antiferromagnetic nearest-neighbor interaction.[5,6] All the hexagonal manganites are known to have ferroelectric transition temperatures higher than 500 K, and they all undergo an antiferromagnetic transition around 100 K.

$YMnO_3$, a typical hexagonal manganite, shows an antiferromagnetic transition at $T_N=75$ K and a ferroelectric transition at $T_C=913$ K.[7] Because of the 2D edge-sharing triangular network of the Mn moments, neutron scattering data of $YMnO_3$ exhibits clear diffuse scattering even well above T_N.[8] On the other hand, in the antiferromagnetic phase the ordered moments lie in the basal plane with $\mu_{ord}=3.30$ μ_B/Mn at low temperatures, which is a much reduced value from the ionic moment of 4.0 μ_B for Mn^{3+}. In the ordered phase, an angle (ϕ) between the moments and principal crystallographic axis in the ab plane is about 10°,

which corresponds to a mainly Γ_3 representation with a small mixture of a Γ_4 representation.[9] We also note that bulk properties display clear signs of magnetic frustration effect. Most importantly, the antiferromagnetic ordering temperature of $YMnO_3$ is considerably suppressed compared with its Curie-Weiss temperature $\theta_{CW}=-545$ K. A measure of such magnetic frustration defined as the ratio of $f=|\theta_{CW}|/T_N$ (Ref. 10) is as large as 7.8 for $YMnO_3$.

$LuMnO_3$ is another hexagonal manganite with similar transition temperatures, and basically shares all the physical properties of $YMnO_3$, except for the magnetic structure. While the moments lie in the ab plane like $YMnO_3$, the angle ϕ (as defined above) is about 80° between the moments and the principal crystallographic axis in the ordered phase for $LuMnO_3$. Therefore, the magnetic structure of $LuMnO_3$ can be described by a mainly Γ_4 representation with the slight mixture of a Γ_3 representation, which is a reversed case from that of $YMnO_3$.

As regards the origin of the multiferroic behavior of the hexagonal manganites, we have recently demonstrated with high-resolution neutron-diffraction studies that both $YMnO_3$ and $LuMnO_3$ exhibit very large atomic displacements below the Neel points.[11] We particularly emphasized the importance of the temperature dependence of Mn x position in understanding the coupling between the moments and the polarization. Based on the experimental observations, we proposed a scenario for the multiferroic property of the hexagonal manganites; a strong spin-lattice coupling induces the observed gigantic atomic displacement triggered by the change in the Mn x position. This would then lead to the coupling between the magnetic moments and the electric polarization, i.e., multiferroic behavior. This large magnetoelastic phenomenon, more specifically the big atomic displace-

ment of the Mn x position induced by the antiferromagnetic transition was also recently confirmed for other hexagonal manganites such as HoMnO$_3$, YbMnO$_3$, and ScMnO$_3$.[12]

In this paper, we have undertaken a detailed investigation into doping effects over the entire concentration of (Y,Lu)MnO$_3$ by measuring bulk properties such as susceptibility and heat capacity. We have also made high-resolution neutron-diffraction studies on all together five different samples over a wide temperature range from 10 to 1200 K in order to further examine the proposed spin-lattice coupling as well as the 2D ordering of the Mn moments. Moreover, we have carried out local spin-density approximation (LSDA) band calculations on both YMnO$_3$ and LuMnO$_3$ for better understanding of the experimental results. We should also mention particularly attractive features of (Y,Lu)MnO$_3$ as doping studies: (i) the magnetic framework of Mn atoms remain unchanged with doping, except for the expected chemical pressure effect depending on the relative ionic size of Y and Lu and (ii) since both Y and Lu are nonmagnetic elements there is no magnetic contribution other than that from the Mn moments. Therefore, the doping study of (Y,Lu)MnO$_3$ is a clean way of exploring the interesting magnetic properties of the hexagonal manganites.

II. EXPERIMENTAL DETAILS

We prepared five (Y$_{1-x}$Lu$_x$)MnO$_3$ samples with $x=0$, 0.2, 0.5, 0.7, and 1 using Y$_2$O$_3$, Lu$_2$O$_3$, and Mn$_2$O$_3$ of 99.999% purity (analytical reagent grade) by the standard solid-state reaction method. All the starting materials were mixed and ground several times in order to produce homogeneous mixture. Final sintering was made at 1300 °C for 24 h with several intermediate grindings. Subsequent x-ray diffraction measurements with D/MAX-2200 Ultima (Rigaku) showed that all the samples had no trace of impurities phases, and their measured patterns could be indexed according to the $P6_3cm$ space group of the hexagonal manganites. With increasing Lu concentration, we observed that the lattice constants and the unit-cell volume changed linearly following the Vegard's law. We also measured magnetization from 2 to 300 K using a commercial superconducting quantum interference device magnetometer (Magnetic Property Measurement System MPMS-5XL, Quantum Design) under magnetic field of 100 Oe, and heat capacity from 2 to 250 K using a commercial cryostat (Physical Property Measurement System PPMS9, Quantum Design).

Neutron-diffraction measurements were carried out on all five samples from 10 to 300 K with a wavelength of λ =1.835 Å and the angular cover of $2\theta=10°-160°$ using the high-resolution powder diffractometer (HRPD) at the Korea Atomic Energy Research Institute. To understand further the temperature dependence of the crystal structure, in particular, the question of the spin-lattice coupling, we have extended our measurements up to 900 K and 1200 K for LuMnO$_3$ and YMnO$_3$, respectively. All the diffraction data were analyzed using the FULLPROF program.[13]

III. RESULTS AND ANALYSIS

Figure 1 shows both inverse susceptibility and heat capacity for all the five samples. As one can see in the figure, the
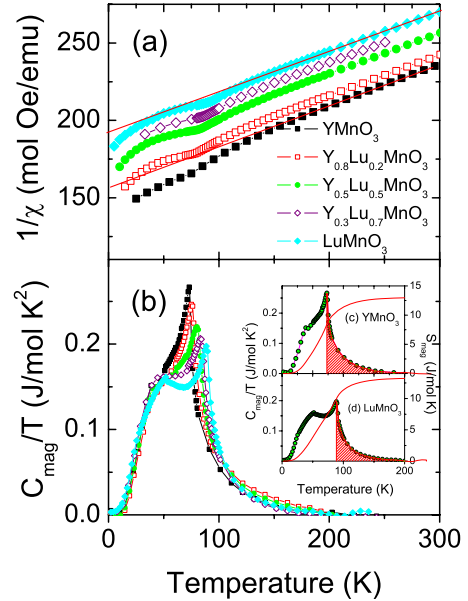

FIG. 1. (Color online) The temperature dependence of (a) inverse susceptibility and (b) magnetic heat capacity is shown for Y$_{1-x}$Lu$_x$MnO$_3$. The antiferromagnetic transition points (T_N) are indicated by the peaks in the magnetic heat capacity for Y$_{1-x}$Lu$_x$MnO$_3$ ($x=0.0$, 0.2, 0.5, 0.7, and 1.0). Lines in (a) correspond to fitting results with the Curie-Weiss formula for YMnO$_3$ and LuMnO$_3$. The insets in (b) show the total magnetic entropy (S_{mag}) as function of temperature for YMnO$_3$ and LuMnO$_3$. The integration of the shaded area corresponds to S_{mag} released in the paramagnetic phase.

inverse susceptibility is almost linear in the paramagnetic phase before showing a weak but clear anomaly at T_N. Representative fitting results with the Curie-Weiss law are shown in the figure for two compositions: YMnO$_3$ and LuMnO$_3$. The inverse susceptibility has almost the same slope in the paramagnetic phase for the five samples. It demonstrates that the effective moment (μ_{eff}) is very similar for all the samples as expected since Mn has the same 3+ valence regardless of doping. A quantitative estimation of the effective moment was made on the experimental data using a Curie-Weiss law in addition to constant background for paramagnetic contribution with the results summarized in Fig. 2(c). The slightly larger value of the experimental effective moment compared with the theoretical value might as well arise from a g factor being larger than an ideal value of 2 for a spin only case. Simultaneously, the Curie-Weiss temperature (θ_{CW}) gets increased continuously with increasing Lu concentration as demonstrated in the experimental data that the inverse susceptibility appears to be shifted upward although they are plotted without any arbitrary adjustment. For example, the Curie-Weiss temperature increases from −550 K for YMnO$_3$ to −740 K for LuMnO$_3$.

Magnetic contribution in the heat capacity was estimated from the total heat-capacity data by subtracting off phonon parts with two Debye temperatures:[14] $\theta_D \approx 365-419$ K for heavy elements and $\theta_D \approx 725-885$ K for lighter elements. We then obtained the magnetic heat-capacity data (C_{mag}) as shown in Fig. 1(b). The peak in the magnetic heat-capacity
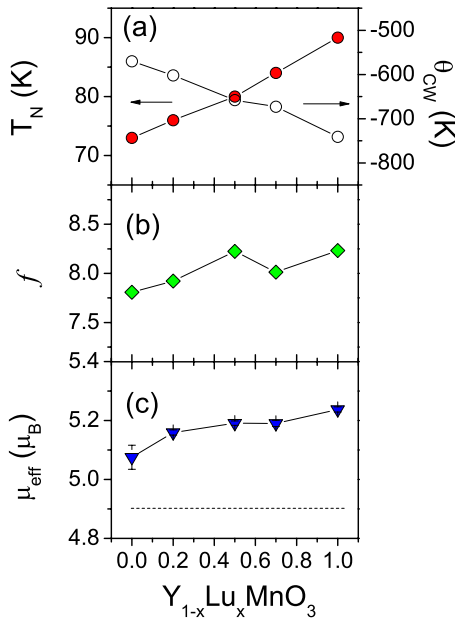
FIG. 2. (Color online) We plot several parameters as function of Lu concentration: (a) the Neel temperature (filled circle) determined from the heat capacity and the Curie-Weiss temperature (open circle); (b) frustration parameter $f (=|\theta_{CW}|/T_N)$; and (c) effective moment (μ_{eff}) together with error bars as obtained from the bulk susceptibility (symbols). The dashed line in (c) corresponds to a theoretical effective moment value of 4.9 μ_B for Mn^{3+} with $S=2$.

data is conspicuously seen, indicative of the Neel temperature. With increasing Lu concentration, the Neel temperature gets increased consistent with the Curie-Weiss temperature determined from the susceptibility data as discussed above. If we take a ratio between the Curie-Weiss temperature and the Neel temperature, then a so-called f parameter ($f=|\theta_{CW}|/T_N$) remains almost the same for the five samples, i.e., doping independent. A summary of the analysis of both susceptibility and heat capacity is given in Fig. 2.

Of further interest, one can also see a shoulder-type structure appearing at lower temperatures apart from the peak at T_N. According to our analysis of inelastic neutron scattering data,[8] it is due to a sudden collapse of a spin gap that takes place well below T_N. Another noticeable feature about the heat-capacity data is that it has a non-negligible magnetic contribution (S_{mag}) above T_N, which extends to very high temperatures, almost three times T_N. See the shaded area in the insets of Fig. 1(b). By integrating the magnetic heat-capacity data up to 200 K, the highest temperature in our measurement, the total magnetic entropy: $S_{mag}=R \ln(2S+1)$ =13.38 J mol^{-1} K^{-2}, of Mn^{3+} with $S=2$ is fully recovered. Moreover, a surprisingly large proportion ($\sim 30\%$) of the total magnetic entropy appears to be released in the paramagnetic phase, which is very unusual for typical magnetic systems. This large entropy released above T_N, we think, is another sign that the Mn moments are magnetically frustrated.

In order to further understand doping effect on the crystal and magnetic structures, we undertook neutron-diffraction measurements for all the samples from 10 to 300 K. We note that our previous high-resolution x-ray and neutron-

diffraction studies confirmed that hexagonal $RMnO_3$ keeps its space group of $P6_3cm$ even when it undergoes the antiferromagnetic transition.[11] Therefore, in the present work we focus on the doping dependence of the magnetic structure. For the $P6_3cm$ space group with a propagation vector $k=0$, there are all together six possible magnetic representations: four of them (Γ_1, Γ_2, Γ_3, and Γ_4) are of one dimensional and the other two (Γ_5 and Γ_6) are of two dimensional. Among the six possible representations, only the four one-dimensional representations appear to be favored by the real materials. Detailed discussion of the magnetic structure is given in Refs. 15 and 16. On passing, we also note that although it is *a priori* possible to have Lu occupying preferentially one of the two possible sites: 2a and 4b sites, our analysis found that within the experimental resolution we cannot distinguish between the ordered and disordered models. Moreover, the difference between Mn-O3 and Mn-O4 bond distances are always present despite the models used, i.e., the difference in bond length is model independent. Thus, in this paper we carried out our analysis using a disordered model of rare-earth sites, i.e., Y and Lu occupying evenly both 2a and 4b sites.

Typical low-temperature data are shown in Fig. 3(a) for all the five compositions with clear signs of the magnetic peaks. Since the hexagonal manganites have distinctive magnetic structures, even a plot like this can be used to examine the doping dependence of the magnetic structure. For example, the magnetic structure of $YMnO_3$ is of a mainly Γ_3 representation with the slight mixing of a Γ_4 representation.[9,15] In this case, the (1 0 0) magnetic peak is stronger than the (1 0 1) magnetic peak as can be seen in the top plot of Fig. 3(a). However, with increasing Lu concentrations a ratio of the intensity of the two strong magnetic peaks becomes reversed and eventually the (1 0 0) magnetic peak almost disappears from the data of pure $LuMnO_3$. Thus even the raw data shown in Fig. 3(a) demonstrate that there is a drastic change in the magnetic structure with doping.

With this information, we have then constructed a magnetic model of a mixed Γ_3 and Γ_4 representation, a magnetic space group of $P6_3'$. Although as far as refinements are concerned a similar mixing of the Γ_1 and Γ_2 representations can be almost as good a model, we discarded it for the reasons as discussed in Ref. 9. Using the mixed model of the Γ_3 and Γ_4 representations, we have obtained the temperature dependence of the magnetic moments for all the samples as shown in Fig. 3(b). During the whole refinement procedures, we achieved good agreement factors for all our data: the overall agreement factors of the refinements are better than $\chi^2=3.6$, $R_p=6.0\%$, and $R_{wp}=7.5\%$ for all the samples. See Table I for the summary.

As one can see in Fig. 3(b), the ordered magnetic moments at low temperatures are almost unchanged independent of doping, although they exhibit higher transition temperatures with increasing Lu concentration. We note that the ordered moment value remains at ~ 3.3 μ_B, smaller than the ionic value of 4 μ_B for Mn^{3+}. Therefore, there is about 0.7 μ_B of the Mn moments still fluctuating at 10 K for all the compounds. On the details of the magnetic structure, the angle (ϕ) between the moments and the principal crystallographic axes is about 10° for $YMnO_3$. With Lu doping this
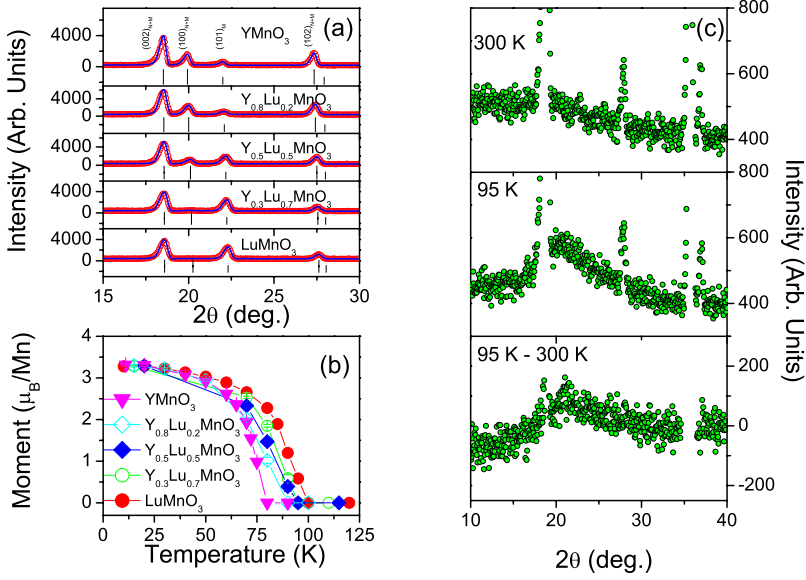
FIG. 3. (Color online) (a) Neutron-diffraction patterns taken at 10 K with observed (circle) and calculated (line) neutron-diffraction patterns for five samples. In order to refine the data, we used the space group $P6_3cm$ and a magnetic model of a mixed $\Gamma_3+\Gamma_4$ representation. The bars indicate the position of the nuclear (upper) and magnetic (lower) Bragg peaks. (b) The temperature dependence is shown of the ordered magnetic moment for the five samples. (c) For $Y_{0.5}Lu_{0.5}MnO_3$, it shows the raw data taken at (top) 300 and (middle) 95 K together with (bottom) the difference between the two sets of the data.

angle (ϕ) gets increased continuously and eventually becomes 83.6° for LuMnO$_3$. Figure 4 summarizes the doping dependence of ϕ, μ_{ord}, and the lattice parameters obtained from the analysis of the 10 K data. That there is a continuous variation in the magnetic structure from the Γ_3 to Γ_4 representations is consistent with our previous observation:[11] the Mn x position changes from $x=0.340$ for YMnO$_3$, larger than 1/3 for an ideal triangular lattice of Mn, to $x=0.331$ for LuMnO$_3$, smaller than 1/3. A similar observation of the correlation between the Mn x position and the magnetic structure was also recently reported for HoMnO$_3$, YbMnO$_3$, and ScMnO$_3$.[12] For the sake of discussion later on, we note that a and c axes contract at different rates with increasing Lu concentration, which is basically chemical pressure effect. We will compare this chemical pressure effects with real pressure effects later in discussion.

In order to examine in the present data the doping dependence of the Mn x position as well as the Mn-O bond distance, we have plotted the data points for 300 and 10 K for all the samples in Fig. 5. For comparison, we have also shown the data obtained from the previous high-resolution measurements.[11] Please note that the powder diffractometer (HRPD of the KAERI) used in this study has an overall resolution of $\Delta d/d \sim 0.3\%$, which is worse by a factor of 4

than the instrument (SIRIUS of the KEK) employed in Ref. 11 with a typical resolution of $\Delta d/d \sim 0.09\%$. Despite the relatively poor resolution of the current data, nevertheless we can still see a clear tendency that the Mn x position gets continuously smaller with increasing Lu concentration while crossing the critical value of $x_c=1/3$ in which the Mn moments form a perfect triangular network. Similarly, Mn-O3 bond becomes relatively smaller with respect to Mn-O4 bond with Lu doping. This subtle change is a key to the doping dependence of the magnetic structure.[11,12]

In order to further investigate the spin-lattice coupling, we have measured the temperature dependence of neutron-diffraction patterns on both YMnO$_3$ and LuMnO$_3$ up to 1200 K and 900 K, respectively. The measured unit-cell volume is plotted over the entire temperature range for both samples in Fig. 6. Note that the reported ferroelectric transition temperatures (T_C) of YMnO$_3$ and LuMnO$_3$ are marked by arrows in both figures. We used the known paraelectric phase of $P6_3/mmc$ for the analysis of the high-temperature data taken above T_C. As one can see in the plot, however there is no visible sign of the ferroelectric transition in the temperature dependence of the unit-cell volume.

For further analysis of the data, we used a Debye-Grüneisen (DG) model.[17] In this model, the temperature de-

TABLE I. Summary of the refinement results of neutron-diffraction data taken at 300 K using the space group $P6_3cm$. Equivalent pressure values (P_{Eq}) are calculated by using the experimental compressibility $k_i=-1/a_{i0}(da_i/dP)_T$, when $a_i=a$, c, and V with $k_a=0.0027$, $k_c=0.0019$, and $k_V=0.0073$ GPa^{-1} (Ref. 30).

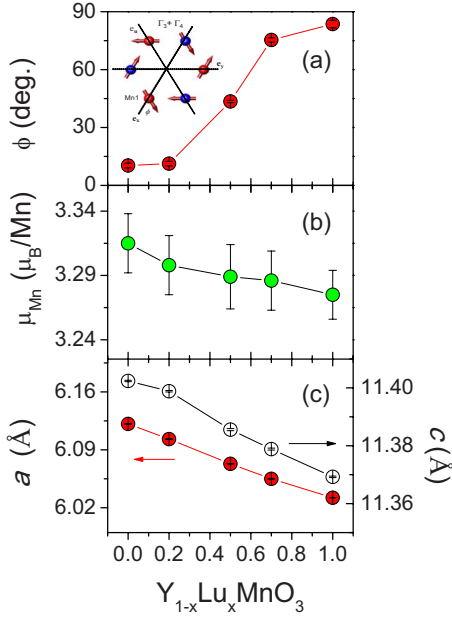|	Crystal parameters						Agreement factors		
$(Y_{1-x}Lu_x)MnO_3$	a (Å)	P_{Eq} (GPa)	c (Å)	P_{Eq} (GPa)	V (Å^3)	P_{Eq} (GPa)	R_p (%)	R_{wp} (%)	χ^2
0.0	6.1392(1)	0.00	11.3913(2)	0.00	371.83(1)	0.00	4.67	6.26	1.72
0.2	6.1208(1)	1.11	11.3880(2)	0.15	369.49(1)	0.86	3.52	4.75	1.80
0.5	6.0899(1)	2.98	11.3790(3)	0.57	365.48(2)	2.34	5.12	6.60	2.95
0.7	6.0714(1)	4.10	11.3741(3)	0.80	363.10(1)	3.22	3.81	5.06	1.61
1.0	6.0465(1)	5.59	11.3668(2)	1.14	359.90(1)	4.39	4.52	5.82	2.24

FIG. 4. (Color online) We plot as function of Lu concentration (a) the angle (ϕ) between the direction of the Mn moment at the Mn1 position (x, 0, 0) and the [1 0 0] axis, (b) the ordered magnetic moment of Mn, (c) the lattice parameters obtained from the refinement of the neutron-diffraction data at 10 K. The inset in (a) shows a schematic picture of the mixed magnetic structure ($\Gamma_3+\Gamma_4$), where the in-plane hexagonal axes are defined by $\mathbf{e_x}$, $\mathbf{e_y}$, and $\mathbf{e_u}=-(\mathbf{e_x}+\mathbf{e_y})$.
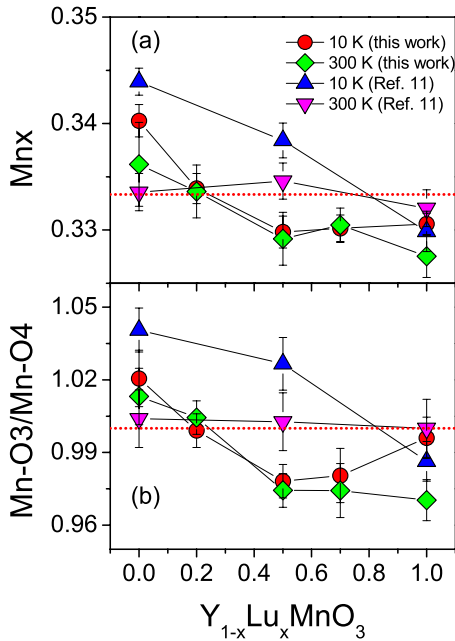

FIG. 5. (Color online) Doping dependence of (a) Mn x position for 10 and 300 K; (b) the ratio between Mn-O3 and Mn-O4 bond distances for 10 and 300 K. For both figures, we have added data points from our previous high-resolution experiments (Ref. 11). The dashed lines correspond to an ideal triangular network of Mn moments.
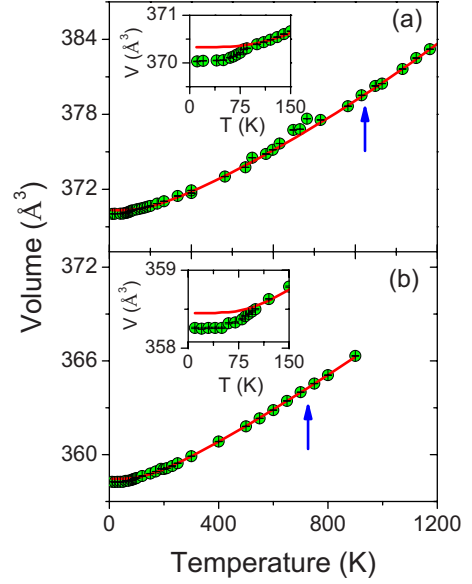

FIG. 6. (Color online) The temperature dependence of the unit-cell volume (symbols) is shown for (a) YMnO$_3$ and (b) LuMnO$_3$ as determined from the refinement results of neutron-diffraction data. Error bars are smaller than the symbol size. The arrows indicate the reported ferroelectric transition while the line corresponds to theoretical curves based on a Debye-Grüneisen model. See the text. The insets in both figures are enlarged pictures of the low-temperature part, where a significant discrepancy emerges between the experimental data and the theoretical curves below T_N.

pendence of the unit-cell volume is given in the following formula at ambient pressure:

$$V(T) = V_0\left[1 + \frac{E(T)}{Q - bE(T)}\right], \quad (1)$$

where V_0 is the unit-cell volume at zero temperature, $Q = (V_0 K_0/\gamma)$, and $b = 1/2(K_0'-1)$. K_0 is the zero-temperature isothermal bulk modulus with K_0' being its first derivative with respect to pressure and γ being the thermal Grüneisen parameter. The internal energy due to lattice vibrations, $E(T)$, is then given by the Debye model,[18]

$$E(T) = \frac{9nk_BT}{(\theta_D/T)^3}\int_0^{\theta_D/T} \frac{x^3}{e^x - 1}dx, \quad (2)$$

where θ_D is the Debye temperature, n the number of atoms per unit cell, and k_B the Boltzmann constant. The solid lines in Fig. 6 are the fitting results using Eq. (1) with the following four constants: for YMnO$_3$, $\theta_D=605$ K, $V_0=370.3$ Å^3, $Q=8.25\times10^{-17}$ J, and $b=6.2$; and for LuMnO$_3$, $\theta_D=580$ K, $V_0=358.5$ Å^3, $Q=8.45\times10^{-17}$ J, and $b=3.2$. We note that a similar approach was successfully applied to other compounds with a similar set of values.[19]

As one can see from Fig. 6, our theoretical curve provides an excellent description of the temperature dependence of the unit-cell volume above the magnetic transition temperature for both YMnO$_3$ and LuMnO$_3$. Upon close inspection, however, a clear deviation emerges between the fitting results and the experimental data below T_N. In order to show this differ-
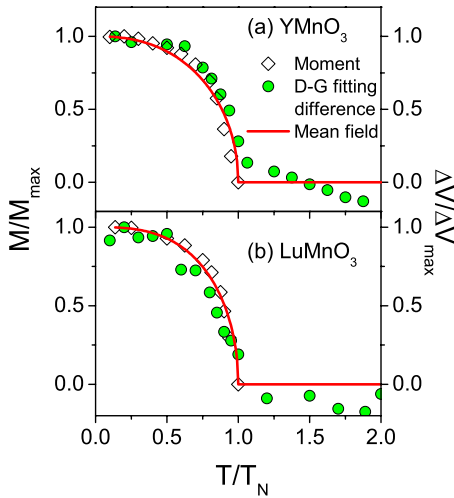
FIG. 7. (Color online) The temperature dependence of the ordered magnetic moment is shown together with the difference in the unit-cell volume (ΔV) as obtained from the DG fitting shown in Fig. 6. The line corresponds to the expected temperature dependence of a mean-field-type order parameter.
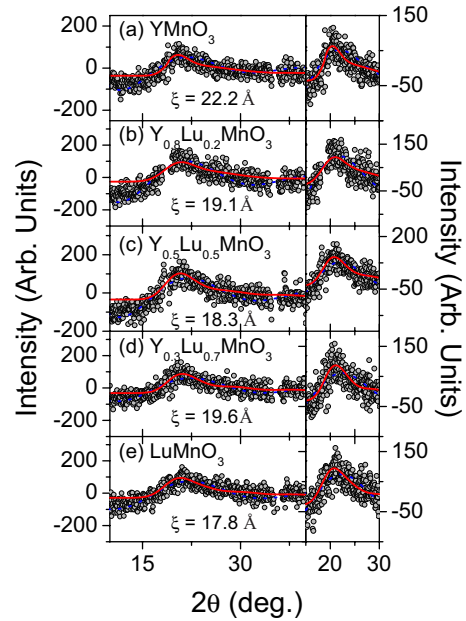

FIG. 8. (Color online) We obtained magnetic diffuse scattering by subtracting off the diffraction pattern taken at 300 K from the raw diffraction patterns at about T_N. The solid lines correspond to the fitting results to theoretical curves for a purely 2D (red solid line) and 3D (blue dotted line) magnetic system. The values of spin-spin correlation lengths (ξ) are shown as obtained from the 2D fitting results.

ence more clearly, we have plotted the low-temperature enlarged pictures of YMnO$_3$ and LuMnO$_3$ as the insets of Fig. 6. Although thermal expansion is typically frozen below the boiling point of liquid N$_2$ for conventional materials, the unit-cell volume of both YMnO$_3$ and LuMnO$_3$ gets significantly reduced below T_N, when compared with the theoretical curve. This difference in the unit-cell volume between the experimental value and the theoretical one, ΔV, is a clear signature of the spin-lattice coupling expected from the previous studies.[11] What is particularly remarkable is that as shown in Fig. 7 this difference (ΔV) in the unit-cell volume seems to exhibit very similar temperature dependence to that of the magnetic moments. Moreover, both data also follows a theoretical curve of mean-field type, $\propto \sqrt{1 - (\frac{T}{T_N})^{1.9}}$. This close agreement observed in the temperature dependence of the volume anomaly (ΔV) and the moments together with the theoretical curve renders stronger supports to our claim that the strong spin-lattice coupling is a driving force that couples the magnetic moment and the electric polarization through the lattice, i.e., a microscopic mechanism for the multiferroic behavior of the hexagonal manganites.

Another interesting point about the hexagonal manganites is that it has large geometrical frustration effects with the 2D triangular network of the Mn moments. As expected, all the bulk properties show clear signs of the magnetic frustration: for example, large f values, ordered moments smaller than the ionic value, and 1/3 of the total entropy released above T_N. An additional signature can also be found in neutron-diffraction data shown in Fig. 8, where strong diffuse scattering appears for all the compositions. In order to get the experimental diffuse scattering data as shown in Fig. 8, we compared the neutron diagrams measured just above T_N with the one at 300 K, and took the difference between the two data sets as our diffuse scattering parts. Since both data were taken under the identical condition bar the temperatures, all the other contributions except for the temperature-dependent

diffuse scattering contributions are presumably the same. Because of the small momentum transfer, i.e., low scattering angles, even the temperature-dependent Debye-Waller factor for the nuclear peaks are also negligible. Our diffuse scattering data contain both elastic and inelastic processes, the latter of which were shown quite strong even in the paramagnetic phase in Ref. 8.

In the previous studies,[8] we reported that based on a three-dimensional (3D) model this diffuse scattering is due to spin clusters pre-existing in the paramagnetic phase, some kind of a preformed magnetic phase of nanoscale. By combining it with thermal-conductivity measurements, we further demonstrated that these fluctuating spin clusters scatter off acoustic phonons strongly, thereby causing a significant reduction in thermal conductivity in the paramagnetic phase.[20] As one can see in Fig. 8, this kind of short-range spin correlation exists for all the materials. To demonstrate how we obtained these data of short-range spin correlation, for Y$_{0.5}$Lu$_{0.5}$MnO$_3$ we have shown in Fig. 3(c) the raw data taken at 300 and 95 K together with the difference data of short-range spin correlation. Although our previous 3D model for the diffuse peak was not too bad in describing the experimental results, nevertheless we notice that it fails to reproduce a particularly asymmetric peak shape as shown in the enlarged picture on the right-hand side. For example, the experimental data rise sharply on the low scattering angle and fall off slowly toward the high scattering angle, which is characteristic of 2D short-range order. To improve the discrepancy, we decided to use a 2D model with a Warren function.[21]

The solid lines in Fig. 8 correspond to the fitting results with the 2D theoretical curves (red solid lines). For compari-

son, results from the previous 3D model are also displayed as blue lines. As one can see, the new 2D model is better at reproducing the asymmetric peak shape, supporting our statement that the spin cluster forms predominantly on the 2D ab plane in the paramagnetic phase. From the fitting results, we estimated spin-spin correlation lengths that vary from 22.2 Å for YMnO$_3$ to 17.8 Å for LuMnO$_3$. This weak decrease in the correlation length with Lu doping appears to be consistent with higher T_N for larger Lu concentration and the magnetic entropy released above T_N, which gets reduced with Lu doping. It is interesting to note that recent optical studies found experimental evidence of a strong spin-charge coupling in hexagonal TbMnO$_3$, implying that the magnetic correlation found in this study facilitates such unusual coupling for other hexagonal manganites too.[22]

IV. THEORETICAL STUDIES: LSDA BAND CALCULATIONS

In order to understand further the experimental observations, we have carried out LSDA band calculations using the data obtained from the previous high-resolution neutron-diffraction studies.[11]

A. Methods

Calculations were performed within the framework of the linear muffin-tin orbitals method[23] using the LSDA. Mn $(4s,4p,3d)$, O $(2s,2p)$, and Y $(5s,5p,4d,4f)$ orbitals were included to the basis set. We carried out integration in the course of the self-consistency iterations over a mesh of 144 k points in the irreducible part of Brillouin zone. We also used a collinear antiferromagnetic ordering, when two out of three Mn ions in one triangular layer have the same spin but the net spin moment for two layers, i.e., a unit cell, is zero.

The exchange constants were computed for the Heisenberg Hamiltonian, which is written in the following form:

$$H = \sum_{i,j} J_{ij} \vec{S}_i \cdot \vec{S}_j \qquad (3)$$

where summation runs twice over every pair (i,j). To calculate the isotropic magnetic interactions, we have implemented the Green's-function method.[24] According to this method, we can determine the exchange interaction parameter between Mn atoms via the second derivative of the total energy with respect to small deviations of the magnetic moments from the collinear magnetic configuration.

The exchange interaction parameters J_{ij} for the Heisenberg model with $S=2$ can be further written in the following form:[24]

$$J_{ij} = \frac{1}{16\pi} \int_{-\infty}^{E_F} d\epsilon \, \text{Im} \sum_{\substack{mm' \\ m''m'''}} (\Delta_i^{mm'} G_{ij\downarrow}^{m'm''} \Delta_j^{m''m'''} G_{ij\uparrow}^{m'''m}), \quad (4)$$

where m (m',m'',m''') is a magnetic quantum number with on-site potential $\Delta_i^{mm'} = H_{ii\uparrow}^{mm'} - H_{ii\downarrow}^{mm'}$ and the Green's-function is calculated in the following way:
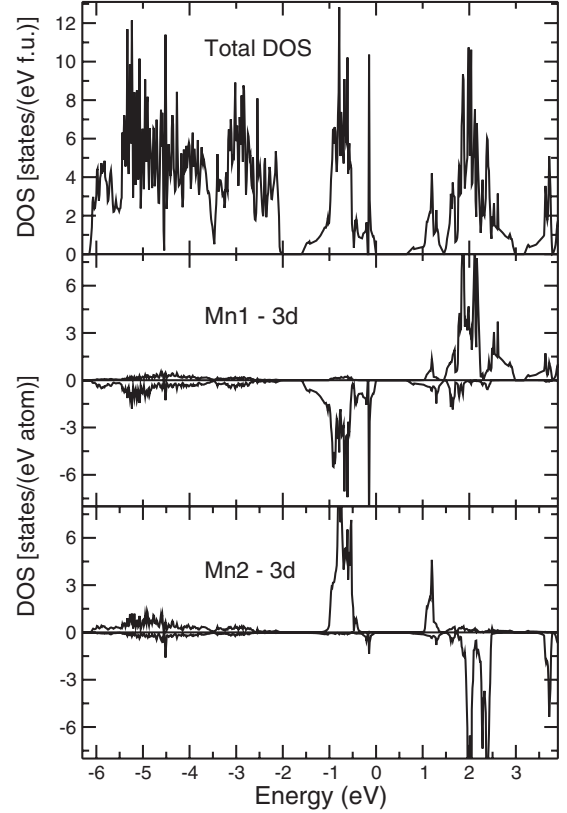

FIG. 9. Total and partial DOS is shown for YMnO$_3$ at $T=10$ K. Mn1 and Mn2 denote ions, which have different directions of spins in one triangular layer. The total DOS is presented as sum over spins while the positive and negative values of partial DOS corresponds to different spins. The Fermi level is at zero energy.

$$G_{ij\sigma}^{mm'}(\epsilon) = \sum_{k,n} \frac{c_{i\sigma}^{mn}(k) c_{j\sigma}^{m'n*}(k)}{\epsilon - E_\sigma^n}. \qquad (5)$$

Here $c_{i\sigma}^{mn}$ is a component of the nth eigenstate and E_σ^n is a corresponding eigenvalue.

B. Exchange interaction

To analyze isotropic exchange interactions between the magnetic moments in YMnO$_3$ we used the crystal structures as determined in the high-resolution neutron-diffraction experiments at 10 and 300 K.[11] The density of states (DOS) obtained in the LSDA for YMnO$_3$ at 10 K is presented in Fig. 9. Due to a strong splitting ∼3 eV between different spin subbands, YMnO$_3$ is an insulator with a band gap of 0.7 eV. This value is about half of the experimental value of 1.27 eV from optical measurements.[25] It is well known that the LSDA method underestimates band-gap values due to a rather rough description of the on-site Coulomb repulsion. More sophisticated approaches, such as L(S)DA+U, can improve it[26] but we should note that our LSDA calculations already provide a correct type of the ground state for this compound.

The results of the exchange constants are summarized in Table II. One can see that the isotropic exchange constant (J)

TABLE II. Exchange constants obtained from LSDA calculations. The distances (d) between Mn ions are presented for the convenience of an analysis. See the text.

	Temperature (K)	J_{intra} (meV)	d(Mn-Mn) intra (Å)	J_{inter} (meV)	d(Mn-Mn) inter (Å)
YMnO$_3$	10	1.55	3.63	2.40	3.49
	300	2.00	3.54	2.10	3.55
LuMnO$_3$	10	2.00	3.44	2.37	3.49
	300	2.25	3.47	2.26	3.47

is sensitive to variations in the Mn-Mn distance. Similarly, the exchange interactions are larger for LuMnO$_3$ than YMnO$_3$ due to a smaller Mn-Mn distance of LuMnO$_3$. Our results demonstrate that at room temperature, where the trimerization is weak, all the exchange constants have similar values for both intraband and interband. However, at $T=10$ K the intertrimer distance (nearest Mn-Mn distance) is not equal to the intratrimer one (next-nearest Mn-Mn distance). This imbalance results in a difference between the corresponding isotropic exchange interactions of J_{intra} and J_{inter}.

Let us discuss further the obtained results in the framework of second-order perturbation theory. Within this theory, the exchange constants can be approximated as $J \propto \frac{\tilde{t}_{dd}^2}{\Delta}$, where $\tilde{t}_{dd}$ is an effective d-d hopping and Δ is an exchange splitting.[27] According to Harrison parametrization,[28] hopping is strongly dependent on distance; $\tilde{t}_{dd} \sim d^{-5}$, where d is a distance between two transition-metal ions. Hence, based on this model the difference in the exchange constants due to the trimerization may be explained by the change in the Mn-Mn bond distances. In fact, a relative change in the Mn-Mn bond distances leads to the decrease of the exchange constants in about 48% for $T=10$ K in YMnO$_3$, while our theoretical calculation shows about 55% difference in the corresponding J values. Thus the change in the J values is mainly due to the difference in the Mn-Mn bond distances, i.e., the chemical pressure effects

Based on the calculated values of the isotropic exchange parameters we can also calculate a theoretical Curie-Weiss temperature using a high-temperature expansion of spin susceptibility: $\theta = \frac{2J_0 S(S+1)}{3}$, where $J_0 = \Sigma_j J_{0j}$ a summation of the exchange constants. We then obtain a theoretical value of Curie-Weiss temperature for YMnO$_3$ ($\theta_{YMnO_3} = 575$ K) in good agreement with the experimental value of about 550 K. A ratio between the Curie-Weiss temperature for both composition (YMnO$_3$ and LuMnO$_3$) becomes $\theta_{YMnO_3}/\theta_{LuMnO_3} = 1.13$ while the corresponding experimental values are ~1.32 (Ref. [11]) and 1.25.[29] Thus, we can see that our LSDA band calculations capture successfully the essential physics of (Y,Lu)MnO$_3$.

V. DISCUSSION AND SUMMARY

As doping experiments, (Y,Lu)MnO$_3$ is a clean system because not only we do not disturb the Mn network by doping at the rare-earth site but also both Y and Lu are nonmag-

netic elements so adding no additional magnetic contribution. Therefore, from the viewpoint of the Mn moments, the only variable is the unit-cell volume, which gets smaller with Lu doping. Can we then understand the whole observed doping effects entirely in terms of chemical pressure effects?

In Table I, we have estimated equivalent pressure values (P_{Eq}) for each composition using the experimental bulk compressibility: $k_a = 0.0027$, $k_c = 0.0019$, and $k_V = 0.0073$ GPa^{-1}.[30] As one can see in the table, there is a stronger change in the ab plane compared with the c axis for a given composition. So the equivalent pressure value for the c axis is smaller than that for the basal plane axis. From the viewpoint of magnetism, this stronger chemical pressure effect seen in the ab plane is rather important since as discussed above the in-plane Mn-Mn exchange interaction is the most important parameter in stabilizing the antiferromagnetic state at low temperatures.

If we use the estimated chemical pressure value (P_{Eq}), then dT_N/dP turns out to be 4.1 and 3.2 K/GPa depending on whether we use the equivalent pressure values for the unit-cell volume or the basal axis. This value is rather close to that obtained from a Clausius-Clapeyron relationship, $dT_N/dP = 2.1$ K/GPa (Ref. [31]) and also the one estimated from pressure-dependent μSR experiments, $dT_N/dP = 2.9$ K/GPa.[32] Therefore, we can state safely that the overall effect of Lu doping can be explained in terms of the chemical pressure effects. On passing, we also note that similar doping and pressure dependences can be found in the rotation angle, ϕ, between the moments with respect to the a axis.[30] It implies that applying either chemical or physical pressure apparently produces a subtle change in the magnetic easy axis. However the energy scale of the magnetic anisotropy in the order of 0.1 meV is too small to be meaningfully captured by theoretical studies likes our band calculations.

With the observed decrease in the ab lattice constant and the in-plane Mn-Mn bond distance, we also expect that the magnetic exchange integral becomes larger for LuMnO$_3$ than YMnO$_3$. In fact, our LSDA band calculation shows an increase in J by $\Delta J = 0.217$ meV at room temperature, a relative increase of 11%. A similar increase in the Curie-Weiss temperature is also expected following the relation: $\theta = \frac{2J_0 S(S+1)}{3}$ According to a theoretical formula for a 2D easy-plane antiferromagnetic Heisenberg model on a triangular lattice,[33] the Neel temperature is also given in the following formula, $T_N \sim 0.3J(S+1/2)^2$. Thus we expect T_N to increase by about the same amount from YMnO$_3$ to LuMnO$_3$, which

is only slightly smaller than the experimental value of $\sim 20\%$.

To summarize, we have demonstrated that with Lu doping at the Y site of $YMnO_3$ we can control the magnetic properties continuously. The continuous variation in the magnetic structure with Lu doping also attests that the magnetic free energy for the Γ_3 and Γ_4 representations is very close to one another. So an even subtle perturbation like Lu doping can be quite critical to preferring one magnetic structure over the other. Our experimental observation together with the LSDA band calculation data support our claim that all the experimental observations can be explained by the chemical pressure effect.

*Present address: Neutron Science Division, Korea Atomic Energy Research Institute, Daejon 305-600, Korea.

†Permanent address: Department of Physics & Astronomy, Seoul National University, Seoul 151-742, Korea; jgpark10@snu.ac.kr

[1] T. Kimura, T. Goto, H. Shintani, K. Ishizaka, T. Arima, and Y. Tokura, Nature (London) **426**, 55 (2003); N. Hur, S. Park, P. A. Sharma, J. S. Ahn, S. Guha, and S-W. Cheong, ibid. **429**, 392 (2004).

[2] W. Eerenstein, N. D. Mathur, and J. F. Scott, Nature (London) **442**, 759 (2006); S.-W. Cheong and M. Mostovoy, Nature Mater. **6**, 13 (2007).

[3] M. Fiebig, J. Phys. D **38**, R123 (2005).

[4] M. A. Gilleo, Acta Crystallogr. **10**, 161 (1957); H. L. Yakel Jr., W. C. Koehler, E. F. Bertaut, and E. F. Forrat, ibid. **16**, 957 (1963).

[5] T. Katsufuji, M. Masaki, A. Machida, M. Moritomo, K. Kato, E. Nishibori, M. Takata, M. Sakata, K. Ohoyama, K. Kitazawa, and H. Takagi, Phys. Rev. B **66**, 134434 (2002).

[6] P. Schiffer and A. P. Ramirez, Comments Condens. Matter Phys. **18**, 21 (1996).

[7] I. G. Ismailzade and S. A. Kizhaev, Sov. Phys. Solid State **7**, 236 (1965); G. Smolenskii and I. Chupis, Sov. Phys. Usp. **25**, 475 (1982).

[8] J. Park, J.-G. Park, G. S. Jeon, H.-Y. Choi, C. Lee, W. Jo, R. Bewley, K. A. McEwen, and T. G. Perring, Phys. Rev. B **68**, 104426 (2003).

[9] J. Park, M. Kang, J. Kim, S. Lee, K.-H. Jang, A. Pirogov, J.-G. Park, C. Lee, S.-H. Park, and H. C. Kim, Phys. Rev. B **79**, 064417 (2009).

[10] A. P. Ramirez, in Handbook of Magnetic Materials, edited by K. H. J. Buschow (North-Holland, Amsterdam, 2001), Vol. 13.

[11] S. Lee, A. Pirogov, M. Kang, K.-H. Jang, M. Yonemura, T. Kamiyama, S.-W. Cheong, F. Gozzo, N. Shin, H. Kimura, Y. Noda, and J.-G. Park, Nature (London) **451**, 805 (2008).

[12] X. Fabrèges, S. Petit, I. Mirebeau, S. Pailhès, L. Pinsard, A. Forget, M. T. Fernandez-Diaz, and F. Porcher, Phys. Rev. Lett. **103**, 067204 (2009).

[13] J. Rodríguez-Carvajal, Physica B **55**, 192 (1993).

[14] D. G. Tomuta, S. Ramakrishnan, G. J. Nieuwenhuys, and J. A. Mydosh, J. Phys.: Condens. Matter **13**, 4543 (2001).

[15] P. J. Brown and T. Chatterji, J. Phys.: Condens. Matter **18**, 10085 (2006).

[16] A. Muñoz, J. A. Alonso, M. J. Martínez-Lope, M. T. Casáis, J. L. Martínez, and M. T. Fernández-Díaz, Phys. Rev. B **62**, 9498 (2000).

[17] D. C. Wallace, Thermodynamics of Crystals (Dover, New York, 1998).

[18] N. W. Ashcroft and N. D. Mermin, Solid State Physics (Harcourt Brace College, Orlando, Florida, 1976).

[19] A. D. Fortes, I. G. Wood, J. P. Brodholt, M. Alfredsson, L. Vocadlo, G. S. McGrady, and K. S. Knight, J. Chem. Phys. **119**, 10806 (2003); S. Lee, J.-G. Park, D. T. Adroja, D. Khomskii, S. Streltsov, K. A. McEwen, H. Sakai, K. Yoshimura, V. I. Anisimov, D. Mori, R. Kanno, and R. Ibberson, Nature Mater. **5**, 471 (2006).

[20] P. A. Sharma, J. S. Ahn, N. Hur, S. Park, S. B. Kim, S. Lee, J.-G. Park, S. Guha, and S.-W. Cheong, Phys. Rev. Lett. **93**, 177202 (2004).

[21] B. E. Warren, Phys. Rev. **59**, 693 (1941).

[22] W. S. Choi, S. J. Moon, B. C. Jeon, J. H. Lee, and Y. S. Lee, J. Korean Phys. Soc. **55**, 754 (2009).

[23] O. K. Andersen and O. Jepsen, Phys. Rev. Lett. **53**, 2571 (1984).

[24] A. I. Liechtenstein, M. I. Katsnelson, V. P. Antropov, and V. A. Gubanov, J. Magn. Magn. Mater. **67**, 65 (1987).

[25] K. Kritayakirana, P. Berger, and R. V. Jones, Opt. Commun. **1**, 95 (1969).

[26] J. E. Medvedeva, V. I. Anisimov, M. A. Korotin, O. N. Mryasov, and A. J. Freeman, J. Phys.: Condens. Matter **12**, 4947 (2000).

[27] It is worth noting that the formula is very similar to the usual superexchange interaction proportional to $\frac{t_{dd}^2}{U}$ while the underlying physics is different.

[28] W. A. Harrison, Elementary Electronic Structure (World Scientific, Singapore, 1999).

[29] T. Katsufuji, S. Mori, M. Masaki, Y. Moritomo, N. Yamamoto, and H. Takagi, Phys. Rev. B **64**, 104419 (2001).

[30] D. P. Kozlenko, S. E. Kichanov, S. Lee, J.-G. Park, V. P. Glazkov, and B. N. Savenko, JETP Lett. **82**, 193 (2005).

[31] D. P. Kozlenko, I. Mirebeau, J.-G. Park, I. N. Goncharenko, S. Lee, J. Park, and B. N. Savenko, Phys. Rev. B **78**, 054401 (2008).

[32] T. Lancaster, S. J. Blundell, D. Andreica, M. Janoschek, B. Roessli, S. N. Gvasaliya, K. Conder, E. Pomjakushina, M. L. Brooks, P. J. Baker, D. Prabhakaran, W. Hayes, and F. L. Pratt, Phys. Rev. Lett. **98**, 197203 (2007).

[33] L. Capriotti, A. Cuccoli, V. Tognetti, P. Verrucchi, and R. Vaia, Phys. Rev. B **60**, 7299 (1999).